Excitation functions of the $^{127}I(\pi,\pi xn)$ reactions in the region of the (3,3) resonance

Y. Ohkubo* and N. T. Porile
Department of Chemistry, Purdue University, West Lafayette, Indiana 47907

C. J. Orth and L. C. Liu
Los Alamos National Laboratory, Los Alamos, New Mexico 87545

(Received 18 October 1982)

Excitation functions have been determined for the formation of ten iodine nuclides (^{117}I–^{126}I) in the interaction of 60–350 MeV π^+ and π^- with ^{127}I. The contribution of various reaction mechanisms has been estimated from the systematic features of the excitation functions and isotopic yield distributions with the aid of cross sections obtained for the production of various isobaric xenon nuclides, cross-section results for 500 MeV proton bombardment of ^{127}I, and comparison with Monte Carlo cascade-evaporation calculations. It is found that, with varying importance, mechanisms involving direct neutron knockout, pion inelastic scattering plus evaporation, pion absorption, and pion charge exchange contribute to the observed yields.

[NUCLEAR REACTIONS $^{127}I(\pi^{\pm},\pi^{\pm}xn)$, $x=1-10$, excitation functions (activation), $T_\pi=60-350$ MeV. KI targets. Deduced reaction mechanisms.]

I. INTRODUCTION

With the availability in recent years of intense pion beams, the study of the interactions of energetic pions with complex nuclei has attracted an interest comparable to that of similar proton-induced reactions. The occurrence of pion absorption as well as inelastic scattering and the dominance of the (3,3) resonance at intermediate energies are complexities not found in the interaction of protons with nuclei. The possibility of using both positive and negative pions as projectiles introduces an added dimension in the properties of this probe that is not available for protons.

Most of the nuclear reactions induced by resonance energy pions that have been studied to date fall in one of the following two broad categories: simple reactions, such as single nucleon removal,[1–4] and spallation.[5–10] The single theoretical model with which all the data can be compared is the intranuclear cascade-evaporation (INC) model. The approach used in this model is to treat the interactions of the incident pion as a series of independent collisions with the target nucleons. The pion-nucleon scattering can be either resonant or nonresonant, the former leading to the formation of the Δ isobar. The subsequent decay of the isobar to a nucleon and a pion corresponds to pion scattering, while the decay to two nucleons results in pion absorption. The struck nucleons, in turn, can hit other nucleons resulting, eventually, in the prompt emission of particles and the formation of an excited residual nucleus. This residue decays in a slower second step by particle evaporation. Both phases of the reaction can be treated by the Monte Carlo technique. The most widely used cascade code is the

TABLE I. Reaction mechanisms in pion induced multineutron removal from ^{127}I.

(1) $^{127}I+\pi^+ \rightarrow$	$^{127-x}I+\pi^++xn$	Direct neutron knockout (DKO); inelastic scattering plus neutron emission (ISE)
(2) $^{127}I+\pi^+ \rightarrow$	$^{127-x}I+p+(x-1)n$	Pion absorption plus nucleon emission
(3) $^{127}I+\pi^+ \rightarrow$	$^{127-x}I+\pi^0+p+(x-1)n$	Charge exchange plus nucleon emission (CEX)
(4) $^{127}I+\pi^- \rightarrow$	$^{127-x}I+\pi^-+xn$	DKO, ISE

VEGAS code,[11] originally developed for incident protons but modified for pion reactions by Harp *et al.*[12] in a version called ISOBAR, with additional refinements added by Ginocchio.[13] The evaporation calculation has usually been performed with the DFF code.[14] The agreement between the ISOBAR–DFF predictions and experiment has ranged from good to poor, depending on the type of information being compared, i.e., cross sections, π^+/π^- cross-section ratios, energy spectra, etc., as well as on the target mass region, and the pion kinetic energy.

The current work focuses on a specific subset of pion-induced spallation reactions, i.e., multineutron removal reactions. The target is ^{127}I, for which the $^{127}I(\pi^{\pm},X)^{127-x}I$ cross sections can be determined for $x=1-10$. The possibility of determining as many as ten different cross sections offers a unique possibility to study the evolution of the reaction mechanism with increasing reaction complexity under conditions that are narrowly controlled by the requirement that the products exhibit no net loss or gain of nuclear charge. The various reaction mechanisms likely to be involved in the formation of iodine isotopes are summarized in Table I. Mechanism I actually involves two distinct paths, a one-step direct knockout process, (DKO) and a two-step cascade-evaporation process involving pion inelastic scattering (ISE). The DKO process has been established for the single neutron removal reaction and its signature is a peak in the excitation function in the vicinity of the (3,3) resonance.[1–4,15] The excitation functions of the multineutron removal reactions should provide an indication of the importance of a single step interaction in the increasingly complex processes that occur as the number of emitted neutrons increases.

Mechanism 2 involves pion absorption followed by particle emission. As indicated in Table I, only π^+ absorption can lead to the formation of iodine nuclides. The dependence of σ^-/σ^+, the cross section ratio for π^- and π^+, on mass loss and pion energy permits us to deduce phenomenologically the contribution of this process as a function of these two variables. Additional information on this point may be obtainable from a comparison of the isotopic yield distributions obtained for π^+ and protons. Although the cross sections of the $^{127}I(p,pxn)$ reactions have been determined,[16] the data are sufficiently old that it was thought desirable to remeasure them. We thus report results obtained for 500 MeV protons.

Mechanism 3 involves pion charge exchange scattering. Again, this process can only form iodine products when π^+ are used. The formation of I nuclides then involves the emission of a proton and $(x-1)$ neutrons. This process has a probability comparable to that of the emission of x neutrons and zero protons, which results in the formation of Xe nuclides. We have accordingly measured the cross sections for the production of these nuclides by π^+. The energy and mass dependence of the $\sigma^+(Xe)/\sigma^+(I)$ ratios provides a qualitative measure of the importance of charge exchange and allow us to distinguish between this mechanism and pion absorption. The $^{127}I(\pi^+,\pi^0)$ reaction is of special interest since the charge exchange process is restricted to a fairly narrow range of final states.

The experimental procedure is described in Sec. II and the results presented in Sec. III. Section IV deals with the systematics of the data and with the interpretation of the results in terms of mechanisms. The results are also compared in this section with the ISOBAR-DFF intranuclear cascade code. Our results for the $(\pi,\pi N)$ reaction were published previously.[4]

II. EXPERIMENTAL

The pion irradiations were performed in the P^3 and LEP channels of the Clinton P. Anderson Meson Physics Facility (LAMPF) with π^+ and π^-

TABLE II. Decay properties of iodine and xenon nuclides.

Nuclide	$t_{1/2}$	γ ray (keV)	Abundance (%)
^{126}I	13.0 d	388.6	35
		666.3	34
		27.3 (*K* x ray)	34
^{125}I	60.2 d	27.3 (*K* x ray)	56.5
^{124}I	4.2 d	602.7	61
		27.3 (*K* x ray)	46.8
^{123}I	13.04 h	159.0	82.9
^{122}I	3.6 min	564.0	18
^{121}I	2.12 h	212.5	84
^{120}I	1.35 h	560.4	73
$^{120}I^m$	53.0 min	560.4	100
		614.7	67
^{119}I	19.3 min	257.5	90
^{118}I	14.3 min	605.2	95
$^{118}I^m$	8.5 min	599.8	100[a]
		605.2	100[a]
^{117}I	2.2 min	325.9	100[b]
^{127}Xe	36.41 d	202.8	68.1
^{125}Xe	17 h	188.4	55
^{123}Xe	2.08 h	148.7	49
^{122}Xe	20.1 h	148.8	3.16
		350.1	8
^{121}Xe	39 min	212.5	84

[a]Relative abundance.
[b]Assumed abundance.

TABLE III. Independent production cross sections (mb) of I nuclides from the interaction of ^{127}I with pions.

T_π	60 MeV		100 MeV		120 MeV		140 MeV		180 MeV		210 MeV		250 MeV		300 MeV		350 MeV	
Nuclide	σ^+	σ^-	σ^+	σ^-	σ^+	σ^-	σ^+	σ^-	σ^+	σ^-	σ^+	σ^-	σ^+	σ^-	σ^+	σ^-	σ^+	σ^-
^{126}I	57.3±	152.9±	59.0±	128.2±			62.8±	133.0±	70.5±	145.9±	68.6±	132.9±	65.0±	110.7±	54.3±	105.0±	53.9	82.3±
	6.2	31.0	6.0	9.4			4.4	8.5	3.8	9.3	4.4	9.1	4.4	7.2	3.3	6.8	2.6	5.9
^{125}I	71.5±	215.5±	97.8±	192.7±			80.6±	168.6±	83.3±	127.4±	94.1±	139.0±	69.3±	94.5±	59.7±	71.6±	71.3±	50.6±
	16.0	86.8	17.1	31.6			9.2	20.3	9.4	18.8	11.7	18.1	7.9	13.5	7.2	16.9	9.4	14.3
^{124}I	27.2±	103.9±	61.9±	112.5±			68.0±	88.1±	57.9±	76.9±	48.5±	61.9±	40.4±	51.3±	30.9±	49.3±	30.7±	39.3±
	4.2	23.0	8.8	11.2			6.5	7.6	3.7	6.5	4.1	5.7	3.6	4.4	2.3	4.3	2.0	3.8
^{123}I	31.4±	52.4±	58.5±	104.8±			83.4±	96.5±	64.9±	74.2±	55.9±	58.6±	46.0±	49.2±	29.6±	44.9±	29.8±	34.9±
	6.9	31.1	9.9	6.2			5.2	3.1	3.0	2.3	2.4	2.1	2.4	1.6	2.4	1.5	1.7	1.8
^{122}I	23.6±		42.6±	59.7±			64.5±	59.4±	49.2±	49.5±	39.4±	43.4±	29.6±	33.0±	24.6±	20.8±	22.1±	20.8±
	5.0		10.2	16.1			14.6	14.1	7.9	8.0	8.9	9.8	6.7	7.5	5.6	4.8	5.2	4.8
^{121}I	35.9±	<3.3±	32.8±	32.9±		52.1±	61.0±	53.7±	59.4±	47.1±	56.6±	39.9±	41.2±	30.3±	26.8±	24.6±	23.6±	17.8±
	12.9	1.1	6.4	1.7		2.4	7.8	1.4	4.3	1.8	5.0	1.3	3.8	1.2	2.0	0.7	2.9	1.3
^{120}I	42.6±		29.1±	7.69±	39.7±	17.3±	45.7±	23.3±	46.2±	25.3±	42.0±	22.9±	30.5±	18.3±	21.9±	15.3±	18.9±	11.0±
	9.9		3.5	0.41	1.4	0.8	1.3	0.7	1.3	1.0	2.3	0.7	1.2	0.8	1.0	0.5	1.2	0.8
^{119}I	38.8±		26.6±	1.04±	34.0±	6.4±	33.0±	10.8±	32.4±	13.7±	29.6±	13.5±	22.7±	11.4±	16.8±	9.97±	14.5±	7.05±
	9.1		3.6	0.21	1.7	0.4	1.8	0.4	1.1	0.6	1.8	0.6	1.3	0.5	0.9	0.43	1.0	0.57
^{118}I	19.3±		13.5±	1.43±	16.1±		14.8±	2.94±	13.0±	3.70±	12.8±	4.68±	10.0±	4.05±	7.82±	4.16±	7.24±	2.88±
	4.5		1.9	0.33	0.9		0.6	0.30	0.8	0.25	0.8	0.24	0.6	0.23	0.38	0.22	0.80	0.26
^{117}I	5.7±		8.94±				8.63±		5.36±		5.38±	2.69±	4.32±	2.38±	3.37±	2.03±	3.34±	2.29±
	0.9		1.23				1.27		0.25		0.30	0.44	0.55	0.43	0.27	0.18	0.19	0.56

TABLE IV. Cross sections (mb) for the production of Xe nuclides in the interaction of ^{127}I with π^+.

Nuclide	T_π (MeV) 60	100	120	140	180	210	250	300	350
^{127}Xe	4.71±	1.63±		1.16±	1.83±	1.45±	0.85±	0.87±	1.09±
	1.05	0.40		0.26	0.33	0.21	0.14	0.16	0.13
^{125}Xe	18.2±	13.1±	13.8±	12.3±	9.40±	8.09±	6.78±	5.58±	5.44±
	2.4	1.1	0.8	0.4	0.28	0.29	0.22	0.22	0.18
^{123}Xe	7.81±	18.7±	17.9±	15.3±	12.6±	10.4±	8.50±	8.04±	7.66±
	1.14	2.5	1.0	0.7	0.6	0.7	0.50	0.49	0.58
^{122}Xe	16.3±	11.6±		21.2±	12.2±	7.76±	5.69±	5.62±	4.91±
	4.7	3.3		6.0	2.9	2.68	1.95	2.17	1.27
$^{121}Xe^a$	10.8±	7.66±		14.0±	8.06±	5.12±	3.75±	3.71±	3.24±
	4.2	1.89		6.6	3.59	2.62	1.91	2.00	1.48

[a]Only the 100 MeV datum was measured; other results are based on scaling of the ^{122}Xe cross sections.

ranging in energy between 60 and 350 MeV. The P^3 beams had a momentum bite of ±6% while the LEP beams (60 MeV) had a ±4% bite. Protons were removed from the π^+ beams by differential energy degradation. The irradiations with 500 MeV protons were also performed at LAMPF.

The targets consisted of KI pellets made by compressing the powder to a thickness of ~120 mg/cm^2. They were circular, had a diameter of 1.5 cm, and were mechanically stable and of good uniformity (~2%). The target stack consisted of a pellet surrounded by thin Mylar guard foils and preceded on the upstream side by a beam intensity monitor foil of the same diameter. The identity of the monitor was dictated by the length of the irradiations. Depending on the half-lives of the products of interest, the irradiations had a duration of approximately 7 h, 1 h, or 3 min. The beam intensity in the 3 min runs was monitored by assay of the ^{11}C activity induced in thin carbon foils.[3] For the longer

TABLE V. Independent production cross sections (mb) of I and Xe nuclides from the interaction of ^{127}I with 500 MeV protons.

Nuclide	
^{126}I	59.4±3.6
^{125}I	90.2±8.9
^{124}I	33.7±2.8
^{123}I	41.2±2.5
^{122}I	16.8±2.8
^{121}I	27.2±2.3
^{119}I	15.0±0.9
^{118}I	6.77±0.40
^{127}Xe	1.05±0.12
^{125}Xe	5.47±0.34
^{123}Xe	4.21±0.45
^{122}Xe	2.83±0.59
^{121}Xe	1.45±0.74

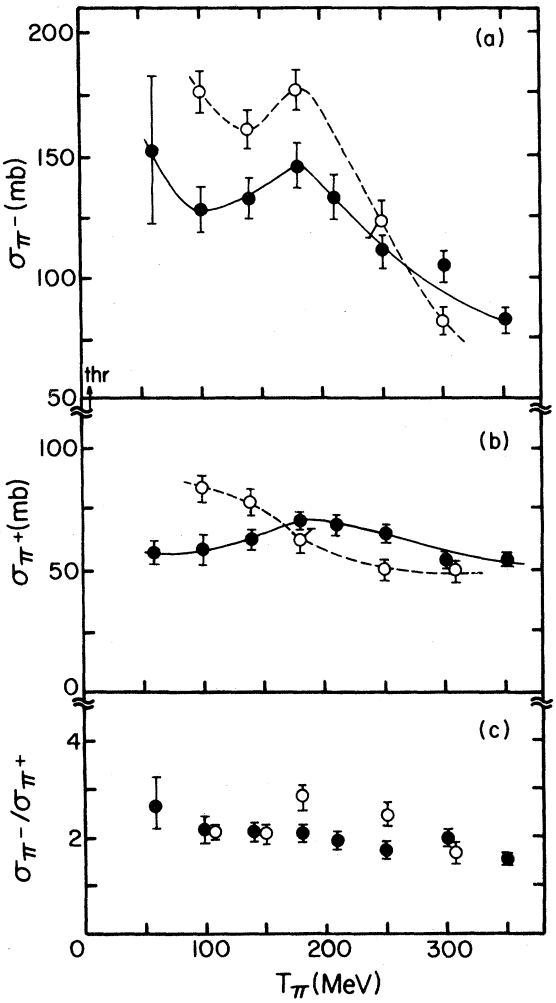

FIG. 1. Excitation functions for the formation of ^{126}I by π^- (top panel) and π^+ (middle panel). Solid points, experiment; open points ISOBAR-DFF calculation. The arrow indicates the reaction threshold for π^-. The lines are drawn to show the trends in the points. The π^-/π^+ cross-section ratios are displayed in the bottom panel.

runs, the beam intensity was monitored by assay of the ^{24}Na activity produced in 120 mg/cm^2 thick silicon discs by means of the Si(π,x)^{24}Na reaction, whose cross sections have been determined.[17] The proton beam intensity was determined by means of the ^{27}Al(p,3pn)^{24}Na reaction.[18] The fluctuations in the pion intensity were monitored by means of a scintillation counter located near the target. The results were corrected by at most 5% for the effect of these fluctuations. Because of the shorter duration of the proton bombardments, no corrections for this effect were made to the proton data.

Following irradiation, the target and monitor discs were separately assayed with calibrated Ge(Li) γ-ray spectrometers, intrinsic Ge x-ray spectrometers, or in the case of the carbon monitor foils, with a NaI annihilation γ-ray coincidence spectrometer. The iodine and xenon products were identified by

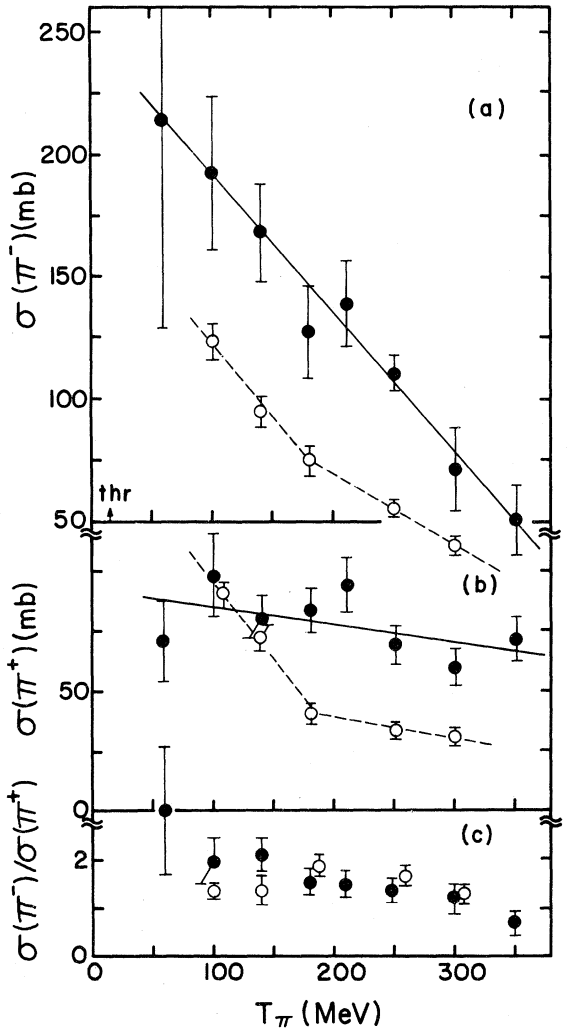

FIG. 2. Excitation functions for the formation of ^{125}I. See Fig. 1 for details.

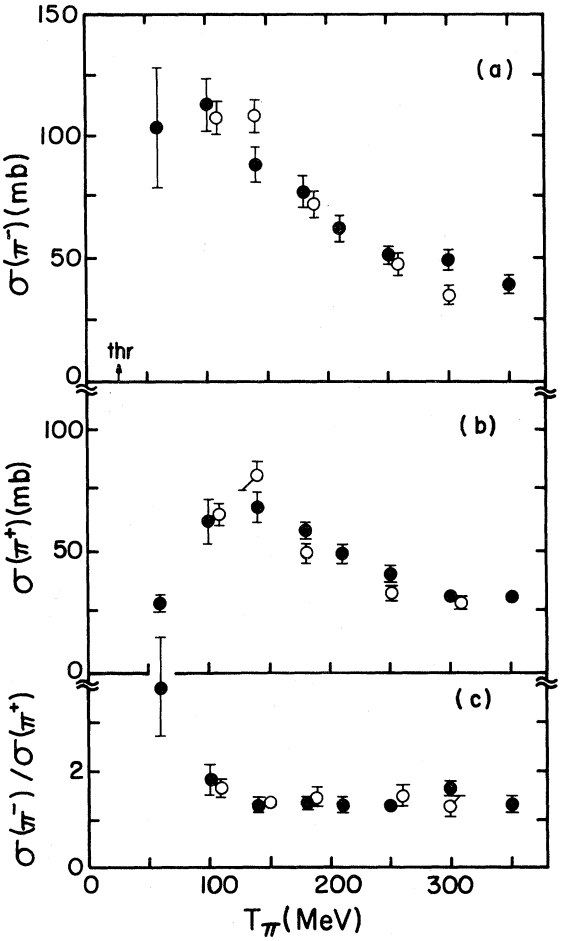

FIG. 3. Excitation functions for the formation of ^{124}I. See Fig. 1 for details.

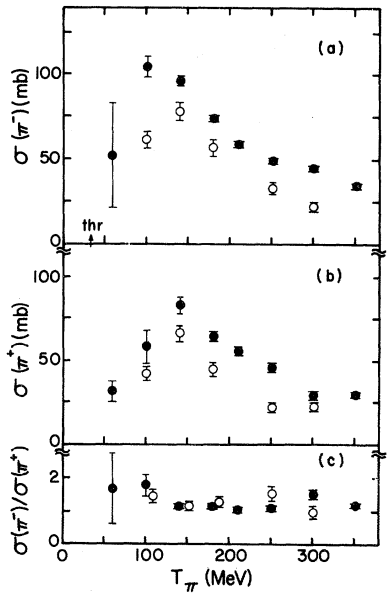

FIG. 4. Excitation functions for the formation of ^{123}I. See Fig. 1 for details.

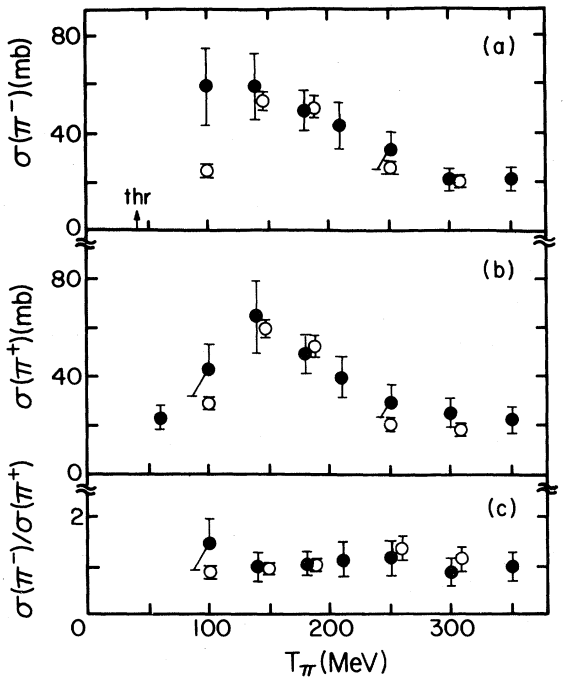

FIG. 5. Excitation functions for the formation of ^{122}I. See Fig. 1 for details.

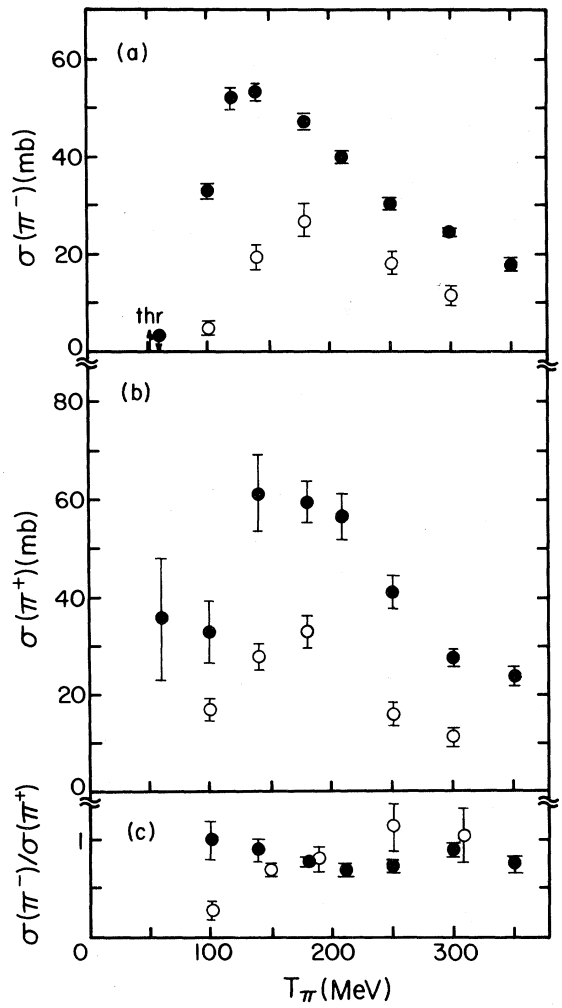

FIG. 6. Excitation functions for the formation of ^{121}I. See Fig. 1 for details.

their characteristic γ rays or x rays and half-lives, as summarized in Table II (Ref. 19). The γ-ray and x-ray spectra were analyzed with the code SAMPO (Ref. 20) and the decay curves were fitted with the CLSQ code.[21] The γ-ray intensities were corrected for γ-γ coincidence summing using a code based on the analysis by McCallum and Coote.[22] This correction amounted to only a few percent in most instances, but to approximately 20% for ^{118}I and ^{122}I due to a combination of high counting geometry and complex level schemes.

Because of a lack of sufficiently intense γ rays, the activity of ^{125}I was assayed by means of the Te K x ray associated with the decay. This same x ray is also emitted in the decay of 58 d $^{125}Te^m$. Since the half-lives of these nuclides are nearly the same, the two activities could not be separated on the basis of gross assay. Accordingly, iodine was radiochemically separated from the long run targets approximately one month after the end of bombardment by means of a standard procedure.[23] The samples were mounted for x-ray assay in the form of AgI pellets. Since there was significant absorption of the x rays by the Ag atoms in the sample, a correction factor had to be applied. This factor was determined by comparison of the x-ray intensity of a carrier-free ^{125}I source with that of a sample in which the same ^{125}I aliquot had been incorporated in AgI. The cross sections determined in this fashion for ^{126}I, which also emits x rays in its decay, were in excellent agreement with those obtained on the basis of γ-ray measurements.

In order to assess the importance of radioactive growth due to the decay of xenon precursors, several runs were performed in which xenon was volatilized from the dissolved samples prior to assay. Comparison of the decay curves of specific γ rays determined with and without this separation was of value in the determination of independent iodine formation cross sections.

The possible contribution of secondary reactions was investigated in experiments performed with 350 MeV π^+ in which the target thickness was varied by a factor of 3. Because of the irradiation conditions, only long-lived products ($t_{1/2} \geq 13$ h) were assayed. From the constancy of the cross sections we conclude that any net secondary contributions to either

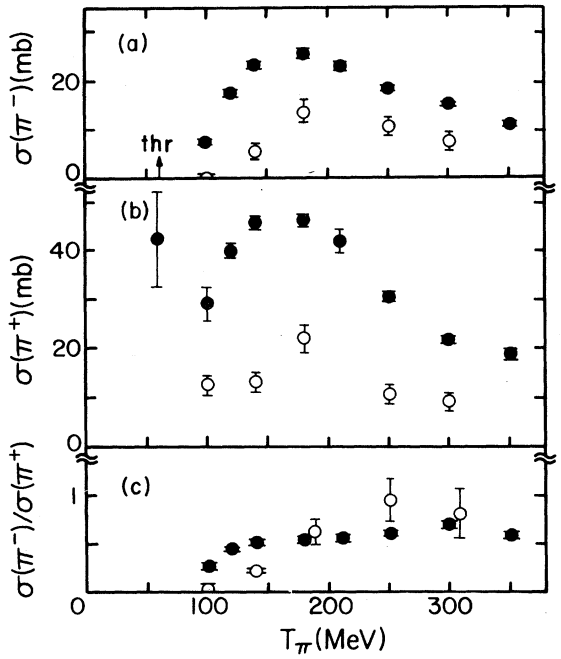

FIG. 7. Excitation functions for the formation of ^{120}I. See Fig. 1 for details.

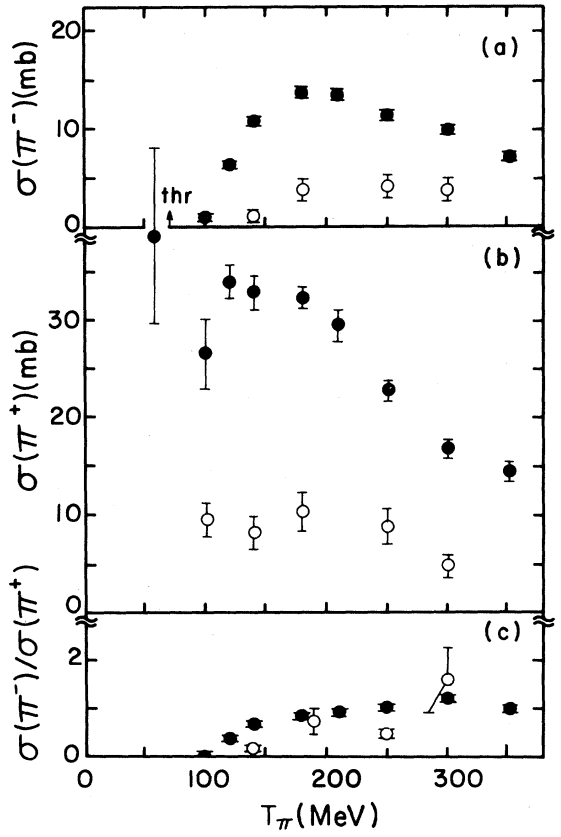

FIG. 8. Excitation functions for the formation of ^{119}I. See Fig. 1 for details.

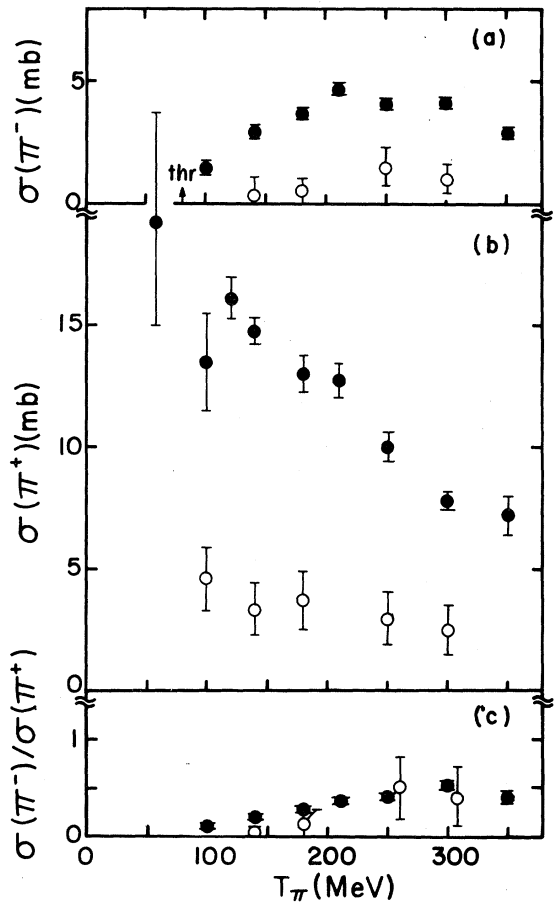

FIG. 9. Excitation functions for the formation of ^{118}I. See Fig. 1 for details.

target or monitor reactions must be less than 2%. We can therefore reasonably conclude that secondary production is unimportant for all our data excepting the ^{127}Xe cross sections. This nuclide is readily made by low-energy protons in a (p,n) reaction and the secondary effect reaches saturation in thinner targets than those used in this experiment. We estimate an upper limit of 10% for the secondary contribution to the yield of this nuclide. More complete details of the experimental procedure are given elsewhere.[24]

III. RESULTS

The measured cross sections are listed in Tables III–V, where Table III summarizes the results for iodine products, Table IV those for xenon products, and Table V those obtained in 500 MeV proton bombardment. The tabulated uncertainties ($\pm 1\sigma$) are due to those from the SAMPO and CLSQ fits, the γ-ray or x-ray abundances, the various correction factors, and the monitor reaction cross sections,

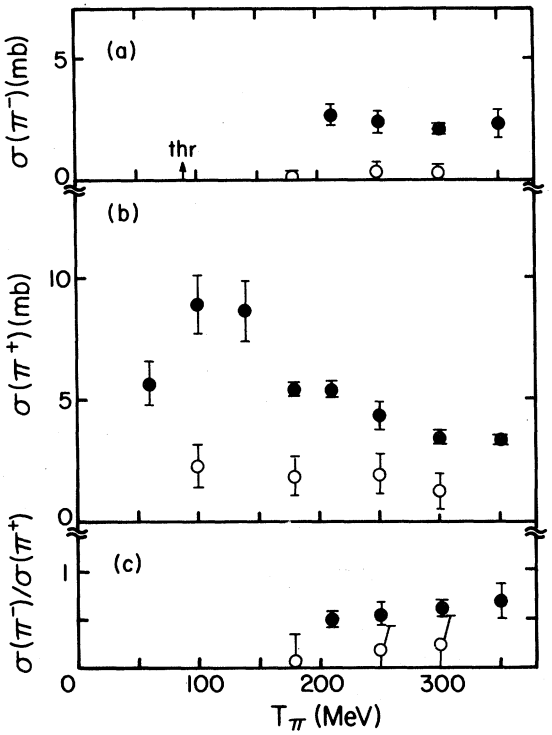

FIG. 10. Excitation functions for the formation of ^{117}I. See Fig. 1 for details.

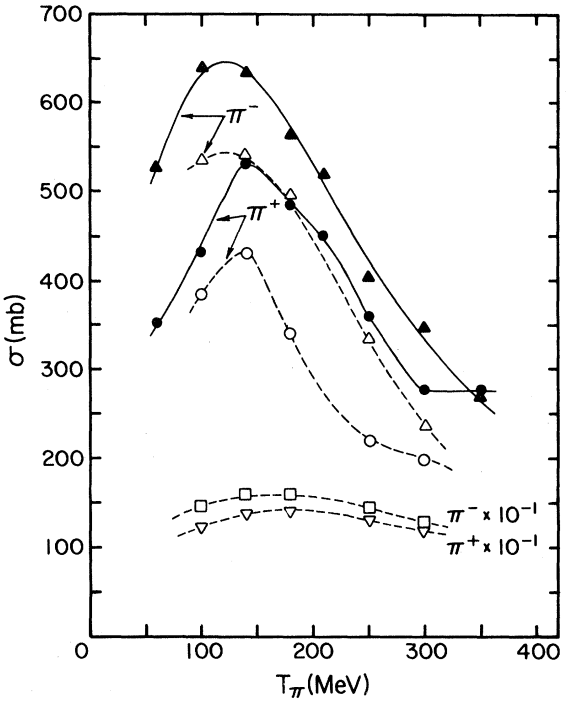

FIG. 12. Energy dependence of the summed iodine cross sections. The solid curves show the trend of the experimental data (●, π^+; ▲, π^-); the dashed curves show the behavior of the ISOBAR-DFF values (○, π^+; △, π^-). The ISOBAR values of the total reaction cross sections σ_R are shown by the dashed curves at the bottom of the figure (▽, π^+; □, π^-). Note that the σ_R values are offset by a factor of 10.

combined in quadrature.

All the tabulated iodine cross sections represent independent yields. In some instances (^{126}I, ^{124}I, ^{122}I) the xenon precursor is either stable or much longer-lived than the irradiation or counting time and consequently no correction was necessary. In other instances (^{120}I, ^{119}I, ^{118}I, ^{117}I) the γ rays of the corresponding xenon precursors could not be detected in the spectra. Furthermore, the decay curves of the γ rays associated with these iodine products showed no evidence of radioactive growth. We conclude on this basis that the contribution of xenon to the observed iodine activities in the above mass range is less than 5%, the cross sections being independent at this level of accuracy. Finally, the decay curves of ^{125}I, ^{123}I, and ^{121}I showed evidence for growth from the decay of the corresponding xenon precursors and the cross sections obtained from the decay data represent cumulative yields. Since the cross sections of ^{125}Xe, ^{123}Xe, and ^{121}Xe could be obtained directly, the tabulated independent iodine cross sections were obtained by subtraction of the corresponding xenon values. It should be remarked in this connection that the ^{121}Xe cross section could only be reliably determined at 100 MeV. The values listed at the other energies were obtained by scaling the ^{122}Xe cross sections by the factor determined at 100 MeV. Since xenon isotopes cannot be formed

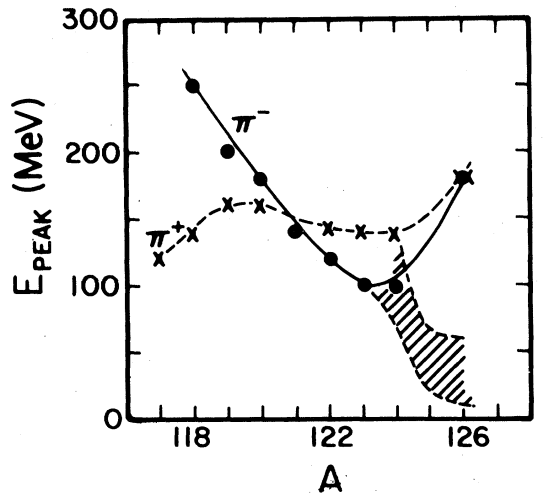

FIG. 11. Peak energies in the excitation functions of neutron removal reactions on ^{127}I. ●, π^- reactions; ×, π^+ reactions. The curves show the trends in the data. The shaded area delineates the energy interval in which the unobserved peaks for ^{126}I and ^{125}I due to the ISE mechanism must lie.

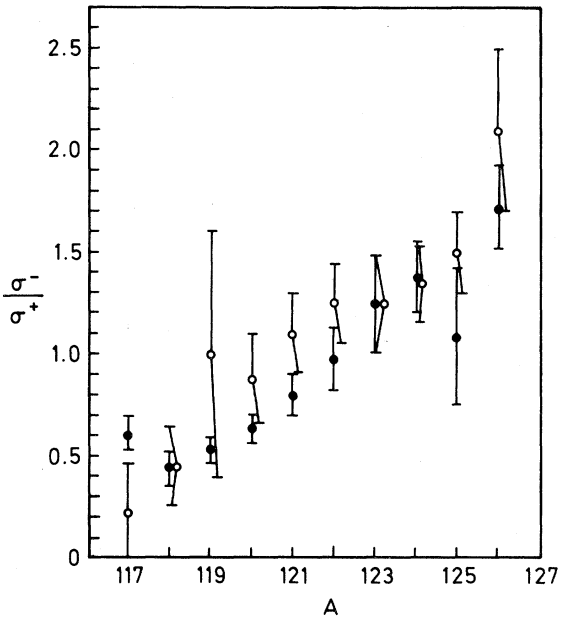

FIG. 13. Mass dependence of the σ^-/σ^+ cross section ratio for iodine nuclides as determined at 250 MeV and higher. Closed points, experiment; open points, ISOBAR-DFF calculation.

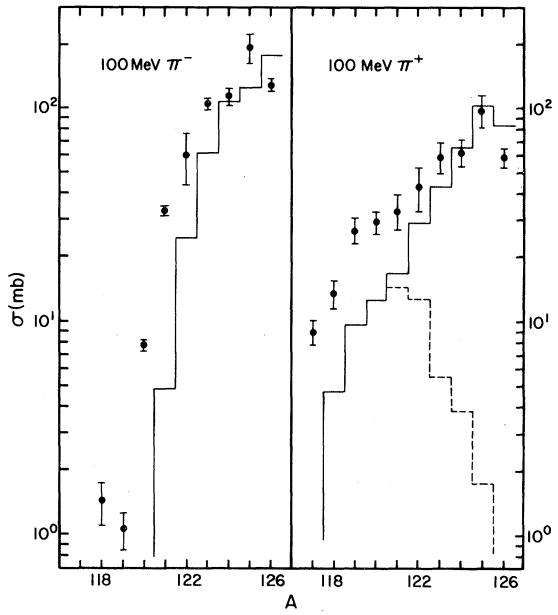

FIG. 14. Isotopic yield distribution of I nuclides obtained with 100 MeV π^+ and π^-. Solid points, experiment; solid histogram, ISOBAR-DFF calculation; dashed histogram, pion absorption contribution to the calculated yield distribution.

by the (π^-, nucleus) interaction (none were detected), the above corrections are only applicable for π^+ and proton bombardment.

The cross sections reported for ^{120}I represent the sum of the measured yields of 1.35 h $^{120}I^g$ and 53 min $^{120}I^m$. The cross sections of $^{120}I^m$ could be directly determined on the basis of the 614.7 keV γ ray. The 560.4 keV γ ray, which is emitted in the decay of both isomers, decayed with a 1.35 h half-life and did not exhibit the growth expected on the basis of the disintegration rate of the 614.7 keV γ ray. The observed results are consistent with an intensity ratio for the 560.4 and 614.7 keV γ rays of $^{120}I^m$ of 0.8, substantially smaller than the value of 1.5 derived from the level scheme.[19] The 560.4 keV decay curve was analyzed on the basis of the experimentally determined intensity ratio.

The 8.5 min $^{118}I^m$ component was not successfully separated from the 600 keV γ-ray activity because the decay curve was unusually complex. On the other hand, the 605.2 keV γ-ray decayed as a single component with the 14.3 min half-life of $^{118}I^g$. The results reported for ^{118}I are based on the assumption that the yield of $^{118}I^m$ is negligible compared to that of $^{118}I^g$.

The results reported for ^{117}I are based on an assumed abundance of unity for the 325.9 keV γ ray. To our knowledge, an absolute abundance has not as yet been reported in the literature. The cross sections of all the other nuclides of interest could be determined in a straightforward manner.

IV. DISCUSSION

A. Excitation functions and cross section ratios

The excitation functions for the $^{127}I(\pi^{\pm},X)^{127-x}I$ reactions are plotted in Figs. 1—10. For each reaction, we display the π^- cross sections, π^+ cross sections, and π^-/π^+ cross section ratios obtained both experimentally and by means of the ISOBAR-DFF code.

The experimental excitation functions vary in a fairly complex yet systematic way with product mass number. Let us first consider the π^- induced reactions. The (π^-,π^-n) reaction displays a peak at the resonance which has been attributed to the DKO process.[4] The increase in cross section observed at the lowest energies reflects the contribution of the ISE mechanism.[4] The calculated cross sections, which exhibit a similar energy dependence, confirm this division according to mechanism.

The (π^-,π^-2n) excitation function, in contrast, decreases monotonically with increasing pion energy over the entire energy regime. There is no evidence for a peak in the vicinity of the resonance. The calculated excitation function displays a similar energy dependence and yields a 1% upper limit for the direct knockout of two neutrons with no subsequent evaporation.

Starting with the (π^-,π^-3n) reaction, all the excitation functions display a peak which shifts to higher energies with increasing number of emitted neutrons and correlates with the reaction threshold. This behavior is expected for a cascade-evaporation (ISE) mechanism and is similar to that observed for (p,pxn) reactions in the same energy regime.[25] The calculated excitation functions for the even-mass isotopes ($A \geq 122$) are in good agreement with the data while those for the odd-mass isotopes are consistently low. This dependence on detailed nuclear properties is suggestive of a deficiency in the evaporation calculation, e.g., incorrect pairing energies. In addition, the calculation consistently underestimates the yields of the lightest iodine nuclides. This discrepancy cannot be attributed to the evaporation code since the calculated probability of proton evaporation is low. Instead, it appears that the ISOBAR cascade code underestimates the probability of pion inelastic scattering involving the emission of only neutrons, once the number of emitted neutrons is seven or more.

A convenient way to display the evolution of the excitation functions is in a plot of peak energy as a function of the number of emitted neutrons, as shown in Fig. 11. The peak energies decrease with increasing mass number as expected from the above considerations. The peaks expected for ^{125}I and ^{126}I lie below 60 MeV, the lowest pion energy for which data are available, and so are unobserved. As mentioned above, the peak observed for ^{126}I at 180 MeV results from a different mechanism and so does not belong on the same curve as the other points.

The excitation functions for the (π^+,π^+xn) reactions are similar to those of the corresponding (π^-,π^-xn) reactions when the number of emitted neutrons is small. The (π^+,π^+n) reaction thus displays a peak at the resonance energy which has been attributed to the DKO process.[4] The (π^+,π^+xn) excitation functions for $x=2-7$ are also similar to the corresponding π^--induced reactions and are consistent with an ISE mechanism.

When the mass loss is larger than seven units, a new feature becomes apparent for π^+ reactions. The trend observed for the peak energies of reactions involving $x=2-7$ reverses itself and the peaks now occur at increasingly lower energies. This trend is most clearly seen in Fig. 11. We believe that the larger cross sections observed at the lower energies reflect a contribution of pion absorption. Recent studies of this process[26] indicate that, for medium to heavy element targets, the cross section for pion absorption attains its highest value in the energy interval of 80 to 150 MeV. This is precisely the regime where the excitation functions in question exhibit their highest cross sections. It is likely, in fact, that the absorption cross section leading to iodine isotopes as the final products has a steeper dropoff at higher energies than the total absorption cross section, since more than just one proton is likely to be emitted at these energies. This behavior accentuates the observed downward shift of the π^+ cross sections. In view of the large energy transfer resulting from pion absorption, a contribution of this process to reactions involving little mass dissipation is unlikely. The excitation functions for the production of the heavier iodine isotopes are therefore similar to those obtained with π^-.

The calculated excitation functions of the (π^+,π^+xn) reactions agree with the data to approximately the same extent as the calculated (π^-,π^-xn) cross sections. The same conclusions about the comparison may be drawn.

The cross sections of the $(\pi,\pi xn)$ reactions may be summed in order to obtain the total yield of iodine isotopes. The resulting excitation functions are plotted in Fig. 12. Included for comparison are values obtained by means of the ISOBAR code. Both experimental and calculated excitation functions peak in the vicinity of 140 MeV. In view of the variation in peak energies discussed above, this value has no particular significance. While the calculated excitation functions have a shape similar to the experimental ones, the magnitudes are substantially lower. This discrepancy has already been noted above.

Total reaction cross sections were obtained from ISOBAR and are also displayed in Fig. 12. The curves have a broad peak in the vicinity of the resonance. The steeper dropoff of the iodine excitation functions indicates that the fraction of σ_R resulting in iodine products decreases with increasing pion energy. At 100 MeV the fractions are thus 0.44 and 0.35 for π^- and π^+, respectively, while at 300 MeV the corresponding values are 0.27 and 0.23. This decrease results from the fact that channels involving additional charge loss become increasingly important at higher energies.

The ratios of π^- to π^+ cross sections are plotted in the bottom panels of Figs. 1—10. For the simpler reactions, the ratios tend to be nearly independent of pion energy. However, for $x \gtrsim 7$, the ratios increase with energy up to perhaps 250 MeV, at which point they become constant. This trend is a reflection of the contribution of the π^+ absorption process to these reactions at low energies.

Since all the ratios appear to be constant at energies of 250 MeV and higher, it is convenient to examine the dependence of the cross section ratios on product mass at these higher energies. Figure 13 displays the average experimental and calculated ratios obtained from the data at 250 MeV and above.

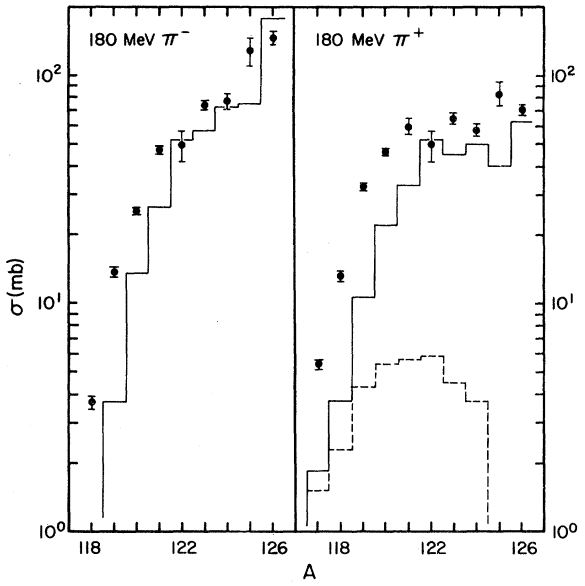

Fig. 15. Isotopic yield distribution of I nuclides obtained with 180 MeV π^+ and π^-. See Fig. 14 for details.

Both experiment and the ISOSBAR-DFF model show that the σ^-/σ^+ ratios decrease with decreasing mass number. This trend can be understood on the basis of the fact that, by virtue of the difference in charge, π^+ tend to favor the formation of more neutron deficient products than π^-. Since the iodine nuclides become increasingly neutron deficient with decreasing mass number, the observed trend follows. The data show that the loss of four or less neutrons is accompanied by larger π^- than π^+ cross sections, while the opposite is the case when six or more neutrons are emitted.

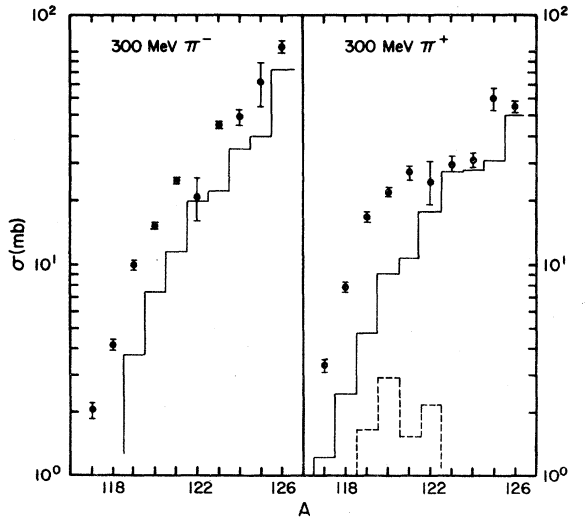

FIG. 16. Isotopic yield distribution of I nuclides obtained with 300 MeV π^+ and π^-. See Fig. 14 for details.

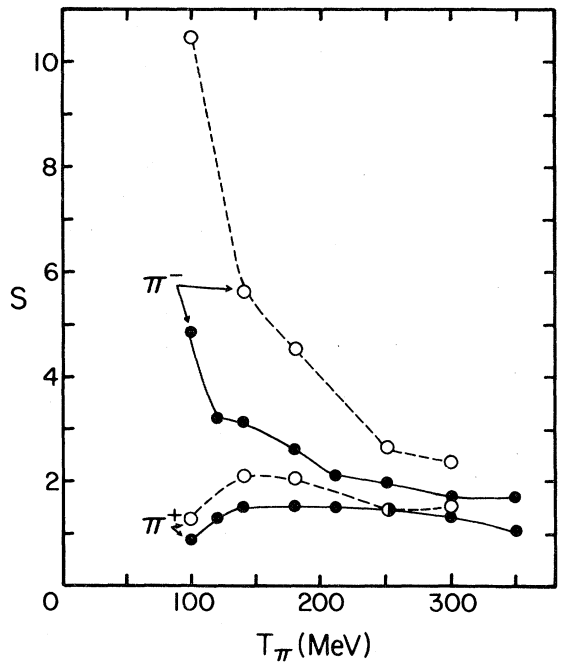

FIG. 17. Slope of the iodine isotopic yield distribution, $S = d\log\sigma/d\log(A\text{-}116)$. Solid points, experiment; open points, ISOBAR-DFF calculation.

B. Isotopic yield distributions

The isotopic yield distributions of iodine nuclides obtained at a few selected energies are displayed in Figs. 14—16. While all the distributions feature a nearly monotonic decrease in cross section with decreasing mass number, some interesting differences may be noted. The distribution obtained for 100 MeV π^+ thus displays a relatively smaller dropoff in yield than the higher energy curves, presumably reflecting the importance of pion absorption in the production of low-mass iodine isotopes at low energies. The π^- distributions drop off more sharply

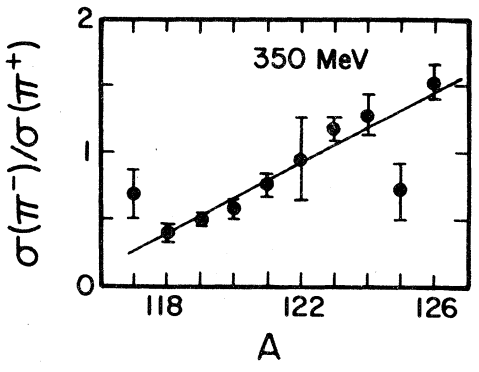

FIG. 18. Mass dependence of the iodine cross section ratio at 350 MeV, designated $R(350)$ in the text. The solid line represents a least-squares fit.

than the π^+ curves at the same energy and the slope of the curves appears to decrease with increasing pion energy. The latter trend is expected for an ISE process in which the amount of excitation energy increases with pion bombarding energy.

Although the cross sections for the formation of products in the vicinity of the target display considerable scatter, the dropoff observed below $A=122$ is more regular. The above trends in this mass region can be quantified in terms of a power law fit to the data. Figure 17 shows a plot of the slope S obtained by a least squares fit to a $\log\sigma$ vs $\log(A-116)$ representation of the data. The difference in the behavior of the isotopic yield distributions obtained with π^+ and π^- is readily apparent in this representation. The effect of π^+ absorption is seen in the increase in slope observed up to ~ 150 MeV. By contrast, the slope of the π^- curve decreases precipitously in this same energy interval. Although the two curves approach each other at the higher energies, the dropoff in yields at low mass numbers is always greater for π^-. This difference presumably reflects the above mentioned effect of the pion charge state on the yield distribution.

The calculated slopes display the same qualitative behavior as the experimental values. However, the actual values are substantially higher than the latter, particularly in the case of π^-. As seen more clearly in Figs. 14–16, this difference means that the calculation severely underestimates the yields of the lighter iodine isotopes.

C. Estimate of the pion absorption contribution

The preceding discussion indicates that π^+ absorption makes a significant contribution to the yield of iodine isotopes at low energies but not at high ones. We can then estimate the contribution of absorption to the yield of the various iodine isotopes as a function of energy on the assumption that at 350 MeV, the highest energy studied, this mechanism does not contribute. The cross section for the formation of some particular isotope by absorption is then estimated by means of the simple expression

$$\sigma_{\rm abs}(\pi^+)=\sigma(\pi^+)-\frac{1}{R(350)}\sigma(\pi^-)\,, \tag{1}$$

where

$$R(350)=\frac{\sigma(\pi^-,350\ \text{MeV})}{\sigma(\pi^+,350\ \text{MeV})} \tag{2}$$

and $\sigma(\pi^+)$ and $\sigma(\pi^-)$ are the experimental cross sections. This procedure assumes that the various factors, other than absorption, that lead to a difference in π^+ and π^- cross sections are independent of energy. This assumption is not strictly correct since, as discussed in the following section, the charge exchange (CEX) contribution to iodine formation decreases with increasing π^+ energy. This factor results in an overestimation of the contribution of absorption to iodine production. However, since CEX makes a relatively small contribution to iodine formation, the error is likely to be small. Furthermore, our procedure also possibly underestimates the absorption cross sections because of the assumption that this mechanism no longer contributes at 350 MeV. The absorption yields will therefore be larger than indicated to the extent that this assumption is incorrect. Since the above two factors work in opposite directions, any errors may cancel.

The values of $R(350)$ are plotted as a function of mass number in Fig. 18. Because there is some scatter in the ratios, we used the fitted line to represent them. The results obtained by means of Eq. (1), expressed as a percent, are displayed in Fig. 19. The contribution of π^+ absorption decreases in a systematic manner with increasing mass number and pion energy. At the lowest energies, π^+ absorption accounts for most of the yield of the lightest iodine isotopes, but by 300 MeV this process no longer appears to contribute to their formation. The absorption yield, summed over all iodine nuclides, is shown as a function of the pion energy in Fig. 20. The most noteworthy feature of this plot is the steep dropoff observed between 100 and 150 MeV.

Figures 19 and 20 also show the absorption yield

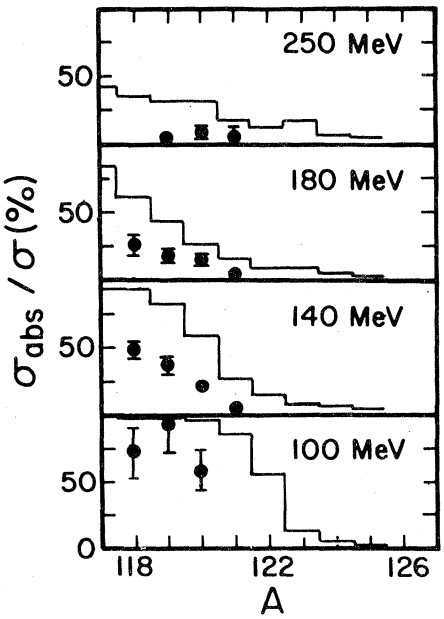

FIG. 19. Percent contribution of π^+ absorption to the yield of iodine isotopes at the indicated energies. Points, obtained from the experimental cross sections by means of Eq. (1); histograms, ISOBAR calculation.

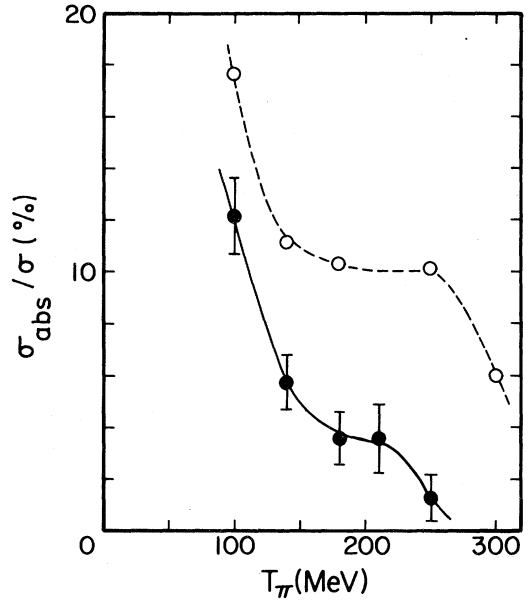

FIG. 20. Energy dependence of the pion absorption yield of iodine products. ●, values derived from experimental cross sections by means of Eq. (1); ○, ISOBAR-DFF predictions.

predicted by the ISOBAR code. While the calculated results display the same qualitative features as the data, the magnitude of the absorption yield is consistently overestimated. This discrepancy may be connected to the fact that the calculation assumes that absorption occurs on a pair of nucleons. If absorption actually involves a larger number of nucleons, and some evidence to this effect has been presented,[27] the resulting distribution of residual nuclei would presumably be affected.

D. Pion charge exchange

The formation of xenon isotopes in reactions induced by π^+ occurs primarily as a result of pion charge exchange, i.e. $(\pi^+, \pi^0 xn)$. The excitation functions for the formation of various xenon isotopes are displayed in Fig. 21. The curves have the shape expected for reactions in which neutrons are emitted either promptly or by evaporation as a result of a cascade involving charge exchange, i.e., a peak that moves to progressively higher energies with increasing neutron loss. The ISOBAR calculation is in generally good agreement with the data.

The isotopic yield distribution of xenon obtained at several energies is compared with the ISOBAR distribution in Fig. 22. Both experiment and calculation show the occurrence of a maximum corresponding to the emission of a few neutrons. The calculated contribution of pion absorption is seen to be rather small, even for the lighter isotopes at low ener-

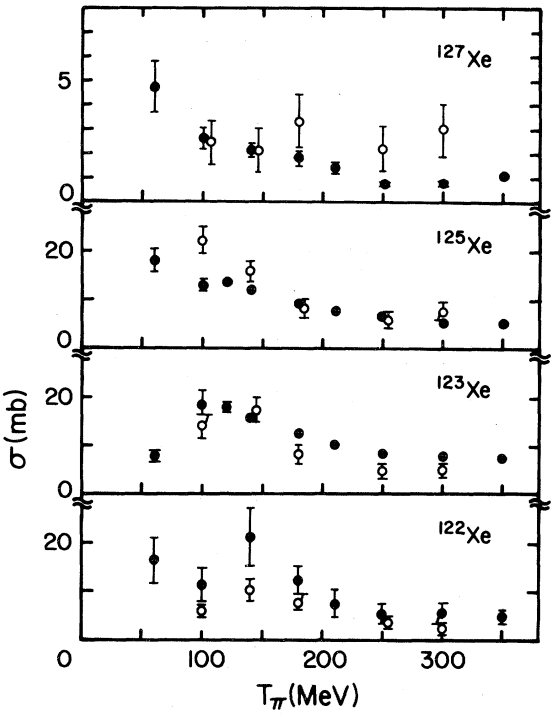

FIG. 21. Excitation functions for the formation of xenon isotopes in π^+ reactions on ^{127}I. ● experiment; ○, ISOBAR calculation.

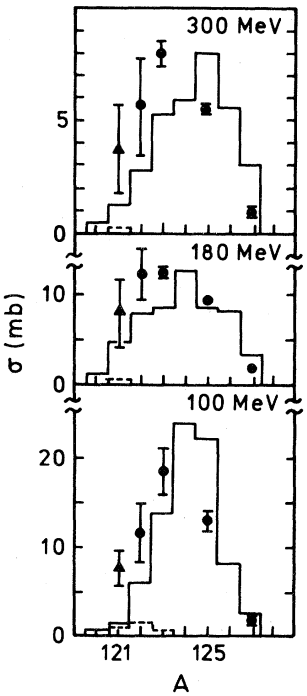

FIG. 22. Isotopic yield distribution of xenon in reactions induced by π^+ with the indicated energies. ●, experiment; ▲, corrected ^{121}Xe cross sections; histogram, ISOBAR calculation; dashed histogram, calculated absorption contribution.

gies. This result is not surprising since the formation of xenon by π^+ absorption requires a second-order process in which an energetic proton undergoes charge exchange on its way out of the nucleus.

An estimate of the contribution of pion charge exchange to the formation of iodine isotopes can be obtained from an examination of the xenon and iodine isobaric yield ratios. We have seen that the production of xenon can occur only as a result of charge exchange, while that of iodine involves a variety of reaction channels. The isobaric yield ratios constitute a valid measure of the CEX contribution to the iodine cross sections to the extent that the emission of one proton and $(x-1)$ neutrons occurs with the same probability as that of x neutrons. Since the probability of proton evaporation is much smaller than that of neutron evaporation because of the high Coulomb barrier in this mass region, the relative contribution of CEX to I and Xe nuclides is determined by the probability of proton emission in the cascade. The ISOBAR model indicates that for a mass loss $\Delta A > 1$ the occurrence of CEX cascades involving the emission of a single proton is of a probability comparable to that of CEX cascades in which no protons are emitted. The isobaric yield ratios consequently constitute a reasonable measure of the CEX contribution to the iodine yields except for ^{126}I.

The isobaric yield ratios, summed over the four isobars $A = 121-123$ and 125, for which both xenon and iodine cross sections are available, are plotted as a function of π^+ energy in Fig. 23. The ratios decrease from approximately 0.3 at 60 MeV to 0.15 at 200 MeV, at which point they level off. The ISOBAR calculation is in good agreement with the experimental values, particularly below 200 MeV. Within the limits of error, all the individual isobaric ratios display a behavior similar to that shown in Fig. 23. The results show that the CEX contribution to the production of iodine nuclides generally amounts to 20% or less. This result is consistent with simple considerations based on the use of free π^+-nucleon cross sections. When two or more nucleons are removed from the target, π^+-p scattering can lead to iodine production in view of the fact that the struck proton can undergo charge exchange. The ratio of isobaric Xe/I cross sections can then be estimated as

$$\frac{\sigma_{\mathrm{Xe}}}{\sigma_I} \simeq \frac{N\sigma(\pi^+ n \to \pi^0 p)}{Z\sigma(\pi^+ p \to \pi^+ p) + N\sigma(\pi^+ n \to \pi^+ n)} \simeq 0.25 ,$$

in approximate agreement with the observed ratio. Note that the single nucleon removal reaction is special in this respect since the CEX contribution to the formation of ^{126}I by π^+ can be as large as 70% (Ref. 15).

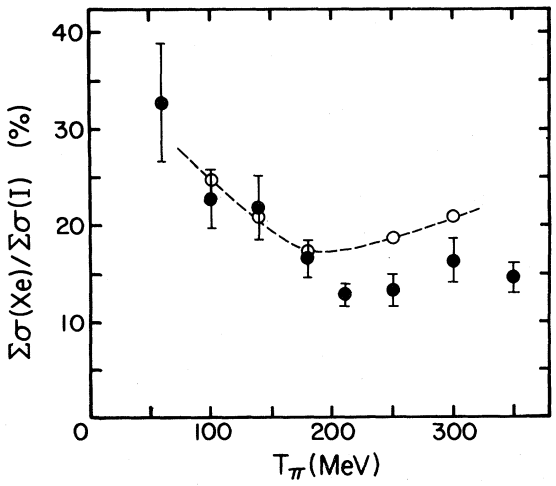

FIG. 23. Ratio of isobaric Xe and I cross sections summed over $A = 121$, 122, 123, and 125. ●, experiment; ○, ISOBAR calculation.

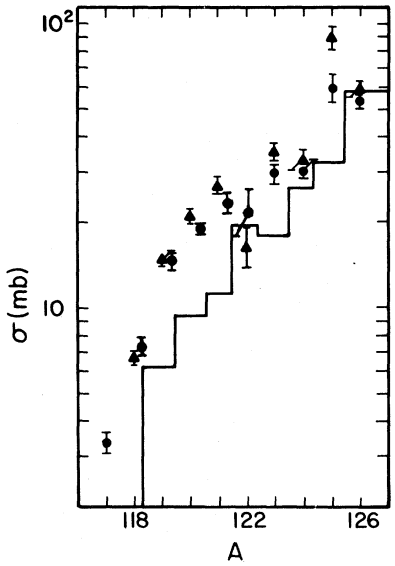

FIG. 24. Comparison of iodine isotopic yield distributions obtained with 500 MeV protons (▲) and 350 MeV π^+ (●). The histogram is the result of the VEGAS-DFF calculation for 500 MeV protons.

E. Comparison with proton results

The iodine isotopic yield distribution obtained with 500 MeV protons is compared with the 350 MeV π^+ results in Fig. 24. Since absorption does not appear to contribute at this high a pion energy, a comparison at the same total projectile energy has no special significance. In view of the fact that the pion excitation functions are fairly flat at the highest energies and as the total reaction cross sections are nearly equal at the energies in question, the

comparison is not inappropriate. The close agreement between the two isotopic yield distributions indicates that the cascade-evaporation process for the two projectiles is quite similar in terms of the distribution of emitted neutrons. Similar qualitative agreement is obtained between the xenon isotopic yield distributions. Also shown in Fig. 24 are the results of a cascade-evaporation simulation run with the VEGAS-DFF code.[11] The underestimation of the yield of the most neutron deficient iodine isotopes is similar to that obtained for pions, and indicates that the problem in the cascade code does not depend on the representation of the π-N interaction.

V. CONCLUSIONS

The excitation functions for the formation of ^{117}I–^{126}I in the interaction of ^{127}I with 60–350 MeV $\pi^{\pm}$ have been determined. Similar results were obtained for a number of isobaric xenon nuclides. An estimate of the contribution of different reaction mechanisms can be made on the basis of these data. The $(\pi,\pi n)$ reaction is the only one for which a one-step direct knockout process (DKO) is of importance. The signature of this process is a peak in the excitation function at the resonance energy. Since the cross sections at both low and high energies remain sizable, it is concluded that a two-step ISE mechanism makes a significant contribution to this reaction. The ISE mechanism is the only one of significance for the other $(\pi^-,\pi^- xn)$ reactions and the principal one for the corresponding π^+-induced reactions.

Two additional mechanisms are of importance in reactions leading to the formation of iodine nuclides induced by π^+. Pion absorption is important for the formation of light products ($\Delta A \geq 7$) at low energies ($T_\pi < 180$ MeV) and accounts for the bulk of the observed yield of these products at 100 MeV. Pion charge exchange appears to make a small ($\sim 10-20\%$) contribution to all the products over the entire energy interval of interest.

The results have been compared with the ISOBAR-DFF cascade-evaporation code. The calculation is generally in qualitative but not quantitative agreement with the data. The most serious failure of the calculation is the consistent underestimation of the yields of light iodine isotopes. It appears that the calculation grossly underestimates the probability of pion inelastic scattering involving the emission of only neutrons, once the number of emitted neutrons is seven or more.

ACKNOWLEDGMENTS

We wish to thank Dr. B. J. Dropesky for facilitating the irradiations and Dr. G. Giesler for his assistance in some of the experiments. This work was financially supported by the U.S. Department of Energy.

---

*Present address: Los Alamos National Laboratory, Los Alamos, NM 87545.

[1]N. P. Jacob and S. S. Markowitz, Phys. Rev. C 13, 754 (1976).

[2]S. B. Kaufman, E. P. Steinberg, and G. W. Butler, Phys. Rev. C 20, 262 (1979).

[3]B. J. Dropskey, G. W. Butler, C. J. Orth, R. A. Williams, M. A. Yates-Williams, G. Friedlander, and S. B. Kaufman, Phys. Rev. C 20, 1844 (1979).

[4]Y. Ohkubo, N. T. Porile, and C. J. Orth, Phys. Rev. C 26, 198 (1982).

[5]B. J. Lieb, W. F. Lankford, S. H. Dam, H. S. Plendl, H. O. Funsten, W. J. Kossler, V. G. Lind, and A. J. Buffa, Phys. Rev. C 14, 1515 (1976).

[6]B. J. Lieb, H. O. Funsten, C. E. Stronach, H. S. Plendl, and V. G. Lind, Phys. Rev. C 18, 1368 (1978).

[7]C. J. Orth, B. J. Dropesky, R. A. Williams, G. C. Giesler, and J. Hudis, Phys. Rev. C 18, 1426 (1978).

[8]H. E. Jackson, S. B. Kaufman, D. G. Kovar, L. Meyer-Schützmeister, K. E. Rehm, J. P. Schiffer, S. L. Tabor, S. E. Vigdor, T. P. Wangler, L. L. Rutledge, R. E. Segel, R. L. Burman, P. A. M. Gram, R. P. Redwine, and M. A. Yates-Williams, Phys. Rev. C 18, 2656 (1978).

[9]S. B. Kaufman, E. P. Steinberg, and G. W. Butler, Phys. Rev. C 20, 2293 (1979).

[10]L. B. Church and A. A. Caretto, Phys. Rev. C 21, 246 (1980).

[11]K. Chen, Z. Fraenkel, G. Friedlander, J. R. Grover, J. M. Miller, and Y. Shimamoto, Phys. Rev. 166, 949 (1968).

[12]G. D. Harp, K. Chen, G. Friedlander, Z. Fraenkel, and J. M. Miller, Phys. Rev. C 8, 581 (1973).

[13]J. N. Ginocchio, Phys. Rev. C 17, 195 (1978).

[14]I. Dostrovsky, Z. Fraenkel, and G. Friedlander, Phys. Rev. 116, 683 (1959).

[15]Y. Ohkubo and N. T. Porile, Phys. Rev. C 25, 2638 (1982).

[16]I. M. Ladenbauer and L. Winsberg, Phys. Rev. 119, 1368 (1960).

[17]R. A. Williams, C. J. Orth, G. W. Butler, G. C. Giesler, M. A. Yates-Williams, and B. J. Dropesky (unpublished).

[18]J. B. Cumming, Annu. Rev. Nucl. Sci. 13, 261 (1963).

[19]*Table of Isotopes*, 7th ed., edited by C. M. Lederer and V. S. Shirley (Wiley, New York, 1978).

[20]J. T. Routti and S. G. Prussin, Nucl. Instrum. 72, 125 (1969).

[21]J. B. Cumming, National Academy of Sciences Report No. NAS-NS-3107, 1962 (unpublished), p. 25.
[22]G. J. McCallum and G. E. Cotte, Nucl. Instrum. 130, 189 (1975).
[23]J. Kleinberg and G. S. Cowan, *The Radiochemistry of Iodine* (National Academy of Sciences—National Research Council, Washington D. C., 1960).
[24]Y. Ohkubo, Ph.D. thesis, Purdue University, 1981.
[25]N. T. Porile, S. Tanaka, H. Amano, M. Furukawa, S. Iwata, and M. Yagi, Nucl. Phys. 43, 500 (1963).
[26]D. Ashery, I. Navon, G. Azuelos, H. K. Walter, H. J. Pfeiffer, and F. W. Schlepütz, Phys. Rev. C 23, 2173 (1981).
[27]R. D. McKeown, S. J. Sanders, J. P. Schiffer, H. E. Jackson, M. Paul, J. R. Specht, E. J. Stephenson, R. P. Redwine, and R. E. Segel, Phys. Rev. Lett. 44, 1033 (1980).